

# ZnSe Nanoparticles for Thermoelectrics: Impact of Cu-Doping

Valeria Demontis <sup>1,\*</sup>, Muhammad Isram <sup>2</sup>, Najaf Abbas Khan <sup>3</sup>, Nasir Amin <sup>3</sup>, Khalid Mahmood <sup>3</sup>   
and Francesco Rossella <sup>2,\*</sup>

<sup>1</sup> Scuola Normale Superiore, NEST Laboratory, Piazza San Silvestro 12, 56127 Pisa, Italy

<sup>2</sup> Dipartimento di Scienze Fisiche, Informatiche e Matematiche, Università di Modena e Reggio Emilia, via Campi 213/a, 41125 Modena, Italy

<sup>3</sup> Department of Physics, Government College University Faisalabad, Faisalabad 38000, Pakistan

\* Correspondence: valeria.demontis@sns.it (V.D.); francesco.rossella@unimore.it (F.R.)

**Abstract:** The present study investigates the impact of copper doping on the thermoelectric properties of zinc selenide (ZnSe) nanoparticles synthesized by the hydrothermal method. Nanoparticle samples with varying copper concentrations were prepared and their thermoelectric performances were evaluated by measuring the electrical transport properties, the Seebeck coefficient, and extracting the power factor. The results demonstrate that the thermoelectric properties of Cu-doped ZnSe nanoparticles are significantly enhanced by doping, mainly as an effect of an improved electrical conductivity, providing a promising avenue for energy applications of these nanomaterials. To gain further insights into the fundamental mechanisms underlying the observed improvements in thermoelectric performance of the samples, the morphological, structural, and vibrational properties were characterized using a combination of scanning electron microscopy, X-ray diffraction, and Raman spectroscopy.

**Keywords:** Cu-doped ZnSe nanoparticles; thermoelectrics; hydrothermal growth



**Citation:** Demontis, V.; Isram, M.; Abbas Khan, N.; Amin, N.; Mahmood, K.; Rossella, F. ZnSe Nanoparticles for Thermoelectrics: Impact of Cu-Doping. *Crystals* **2023**, *13*, 695. <https://doi.org/10.3390/cryst13040695>

Academic Editor: Konstanze R. Hahn

Received: 10 March 2023

Revised: 11 April 2023

Accepted: 12 April 2023

Published: 19 April 2023



**Copyright:** © 2023 by the authors. Licensee MDPI, Basel, Switzerland. This article is an open access article distributed under the terms and conditions of the Creative Commons Attribution (CC BY) license (<https://creativecommons.org/licenses/by/4.0/>).

## 1. Introduction

The rise of global energy consumption and the pressing need to address climate change by reducing greenhouse gas emissions have emphasized the importance of developing sustainable and efficient energy generation and management systems. However, the current low efficiency of energy utilization leads to a significant amount of energy being wasted as heat, which can be recovered and utilized. Furthermore, there is a growing demand for locally available, non-intermittent energy sources to power various devices, including wearable, implantable, and biomedical devices, as well as to manage heat flows in electronic circuits. This need has prompted the intensification of theoretical and experimental studies on thermoelectric energy conversion, which aims to generate usable electrical energy from temperature gradients and potentially convert wasted heat into a valuable resource. Thermoelectric devices, display several advantages, such as the lack of moving parts, which simplifies the design and increases reliability, the possibility to operate in remote or harsh environments, making them suitable for a wide range of applications such as space exploration, automotive and industrial systems. Moreover, they have no emissions and are silent, and have the potential to be highly scalable and easily integrated into existing systems. Despite the current challenges, the scientific community is actively investigating new materials and designs to improve the performance of thermoelectric devices and unlock their full potential. In particular, achieving high thermoelectric figure of merit requires simultaneous optimization of interdependent thermoelectric properties, including electrical conductivity, thermopower, and thermal conductivity. While the efficiency of thermoelectric materials is still relatively low, recent advances in nanotechnology have unlocked significant potential for improving their performance [1]. These include leveraging quantum phenomena and density of states engineering to improve the power

factor [2,3], as well as utilizing nano-structuring to minimize the lattice contribution to thermal conductivity [4,5]. Such techniques have shown great potential for optimizing the performance of thermoelectric materials. More recently, innovative gating approaches have been proposed as a new means of tuning the thermoelectric properties of various semiconductor nanostructures [6].

Group II–VI semiconductor nanostructures have gained considerable attention and are extensively studied due to their diverse range of applications in several fields of technology as well as their unique physical properties [7]. Among them, ZnSe is a widely studied semiconductor with a wide bandgap of 2.7 eV, possessing attractive properties such as eco-friendliness [8], optical transmittance, low resistivity, high electrical conductivity, mechanical hardness, and stability to heat treatment. These properties make it suitable for use in solid-state gas sensors, sensing arrays, photovoltaic cells, and other applications [7]. ZnSe is also used as a buffer layer in copper zinc tin sulfide (CZTS) solar cells instead of CdSe due to its non-toxicity and superior optoelectronic application [9]. In addition, ZnSe has many other applications and properties, including white light emitting diodes (LEDs) [10], optically controlled switches [11], and blue laser diodes [12]. Numerous studies have been conducted on the structural, electrical, and optical properties of ZnSe nanocrystals prepared by different methods, such as chemical vapor deposition (CVD), laser-assisted evaporation (LAE) [13], metal organic chemical vapor deposition (MOCVD), electron deposition (ED) [14], photochemical deposition [15], chemical bath deposition (CBD) [16], and thermal evaporation (TE) [17].

Doping of these nanostructures can significantly enhance their properties, and the use of transition metals, such as  $Mn^{+2}$ , has been extensively studied in various nanocrystalline and nanoparticle materials [18–21]. Among different transition metal doping agents, copper ions ( $Cu^{2+}$ ) are also interesting dopants for ZnSe, as Cu possesses similar electronic shell structure and physical and chemical properties to that of Zn [22]. Thus,  $Zn^{2+}$  ion can be easily replaced by  $Cu^{2+}$ . Literature studies report their role in improving luminescence of ZnSe quantum dots and inducing physical properties such as ferromagnetism addition it also improves the magnetic saturation [23,24].

The objective of the current study was to investigate the effect of copper doping on the thermoelectric properties of zinc selenide (ZnSe) nanoparticles grown by the hydrothermal synthesis method, a topic which has received relatively little attention in previous research. Specifically, the study analyzed the effect of varying copper ion concentrations on the thermoelectric properties of the resulting  $Zn_{1-x}Cu_xSe$  nanocomposites, as well as the role of Cu dopants on the structural, vibrational, and morphological properties of the synthesized nanoparticles. To achieve these objectives, a comprehensive set of experimental techniques was utilized. Initially, the Seebeck coefficient and electrical conductivity of the samples were measured using a standard homemade setup. Subsequently, X-ray diffraction (XRD) and scanning electron microscopy (SEM) were utilized to analyze the structural and morphological properties of the synthesized nanocomposites. Raman spectroscopy was used to gain insights into their vibrational properties.

The results demonstrate that doping and temperature have a significant impact on the thermoelectric properties of ZnSe nanoparticles, particularly through improved electrical conductivity. Additionally, although less pronounced, doping also enhances the Seebeck coefficient, an effect which is not commonly observed. The analysis of the samples' structure and morphology revealed that doping increases defect concentration, reduces crystal size, and leads to the formation of secondary crystal phases. The analysis of the samples structure and morphology revealed that doping increases the defects concentration, reduces the crystal size, and leads to the formation of secondary crystal phases in the material. The reduced crystallinity, likely elevates the significance of grain boundary regions, where the secondary phases are probably located, in determining the thermoelectric properties.

The results of this study contribute to the understanding of the thermoelectric properties of ZnSe nanoparticles doped with Cu and the underlying mechanisms governing their behavior. The findings may have potential applications in the development of

high-performance thermoelectric materials for various energy conversion and harvesting applications.

## 2. Materials and Methods

Copper-doped zinc selenide nanoparticles were synthesized using the hydrothermal method. A first solution of ZnSe was prepared, and different concentrations of Cu (0.1, 0.2, 0.3, and 0.4) were added. Zinc acetate dihydrate ( $\text{Zn}(\text{CH}_3\text{COO})_2 \cdot 2\text{H}_2\text{O}$ , 99% purity, Sigma Aldrich) and selenium (Se, 99% purity, Sigma Aldrich) were separately dissolved in deionized water and mixed together. The necessary amount of copper chloride ( $\text{CuCl}_2$ , 8% purity, Sigma Aldrich) was then added to the aqueous solution of zinc selenide. The pH of the reaction was adjusted to  $8.4 \pm 0.2$  using sodium hydroxide (NaOH, 99% purity, Sigma Aldrich). The precursor solution was stirred for 30 min to obtain a homogeneous mixture. The resulting clear greenish-colored solution of precursors was then transferred into a Teflon-lined stainless steel autoclave with a volume of 50 mL. The autoclave was tightly closed and placed in a hot oven at  $200\text{ }^\circ\text{C}$  for 24 h. Afterwards, the autoclave was allowed to cool down to room temperature and the solution was filtered using filter paper to separate the precipitate. The product was washed with distilled water five times and finally dried in an oven at  $100\text{ }^\circ\text{C}$ . After the synthesis, rectangular pellets of the material were realized by using a hydraulic press having pressure 13 ton [25]. The density of the pellets was found to be around  $2.1\text{ g/cm}^3$ .

The Seebeck coefficient and Power Factor were measured using a homemade Seebeck system, and the electrical conductivity was measured using Hall measurement. The nanoparticles were characterized using various techniques. X-ray Diffraction (XRD) with a Bruker D8 Advanced instrument and a  $\text{CuK}\alpha$  source with a wavelength of 0.145 nm was used to examine the crystalline structure of the sample. Raman spectroscopy was performed using an MN STEX-PR 1100 instrument to analyze the vibration modes. Scanning Electron Microscopy (SEM) with an Emcrafts instrument was used to observe the surface morphology.

To investigate the effect of Cu ion concentration on  $\text{Zn}_{1-x}\text{Cu}_x\text{Se}$  nanoparticles, the molar ratio of  $[\text{Cu}]/[\text{Zn}]$  in the reaction mixture was varied from 0.0 to 0.4 M. The resulting samples were denoted as ZS, CZS1, CZS2, CZS3, and CZS4, and had doping concentration of 0 (undoped), 0.1M, 0.2M, 0.3M, 0.4M, respectively.

## 3. Results and Discussion

### 3.1. Thermoelectric Measurements

The performance at a temperature  $T$  of a thermoelectric material is quantified by the thermoelectric figure of merit  $ZT$  [26], defined by the equation:

$$ZT = \frac{\sigma S^2 T}{k}$$

where  $\sigma$  is the electrical conductivity,  $k$  is the thermal conductivity (which comprises both electronic and thermal contributions), and  $S$  is the Seebeck coefficient, defined as the open-circuit voltage developed across a material in response to an imposed temperature gradient. The numerator of this expression,  $\sigma S^2$ , is known as the power factor,  $P$ , and is a crucial parameter in evaluating a material's thermoelectric properties. A high power factor, combined with low thermal conductivity, is necessary for achieving a high  $ZT$  value.

Figure 1a,b display, for all the samples, the values of the electrical conductivity and of the Seebeck coefficient as a function of temperature.

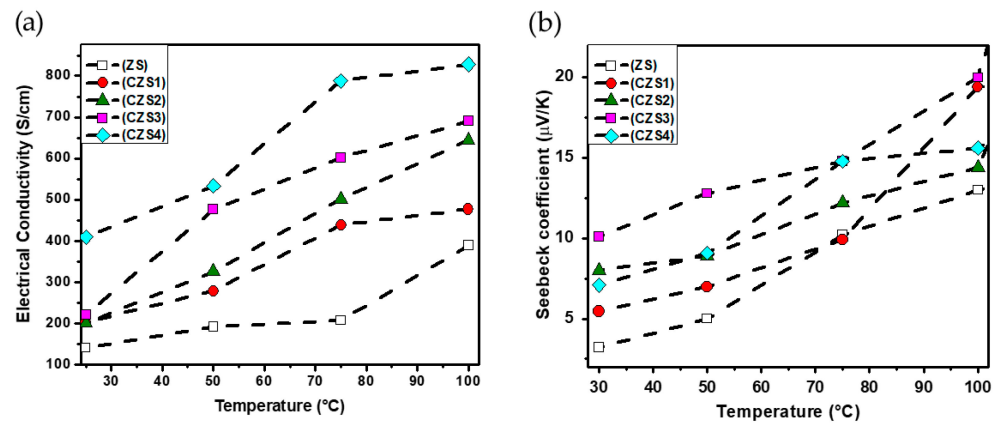


**Figure 1.** Measured values of the electrical conductivity (a) and of Seebeck coefficient (b) for the undoped and Cu-doped ZnSe samples, as a function of temperature.

The undoped sample displayed a typical semiconducting behavior, with an electrical conductivity of about  $140 \text{ Scm}^{-1}$  at room temperature, which increased to about  $390 \text{ Scm}^{-1}$  as the temperature was raised to  $100 \text{ }^\circ\text{C}$ . As expected for doped semiconductors, as the doping concentration was increased, the electrical conductivity of the samples also increased. The electrical conductivity of all the samples increased as the temperature was raised, which is again a common feature of semiconductors. Overall, the results showed that the electrical conductivity of the samples increased from  $140.98 \text{ Scm}^{-1}$  to  $827.99 \text{ Scm}^{-1}$  as the doping concentration and temperature were varied.

The positive Seebeck values indicate holes as the predominant charge carriers, revealing a p-type behavior, in agreement with previously reported literature studies [27].

The Seebeck coefficient exhibits a general increasing trend with both doping and temperature, although its dependence on both factors is not particularly strong. While simultaneous enhancements in Seebeck coefficient and electrical conductivity have been reported several times in the literature [28,29], such occurrences are not common. A comprehensive understanding of the underlying mechanisms and strategies to exploit them for producing high-performance materials is still unknown. Although dedicated theoretical calculations may be required to fully comprehend the physical mechanisms that dictate the specific behavior of the analyzed samples, valuable insights can still be gained by analyzing the morphology and crystal structure of the samples.

The power factor of  $\text{Zn}_{1-x}\text{Cu}_x\text{Se}$  was calculated according to the formula  $\text{PF} = S^2\sigma$ , where  $S$  is the Seebeck coefficient and  $\sigma$  is the electrical conductivity. The graph of the power factor versus temperature, for all the samples, is shown in Figure 2.

The power factor is significantly improved through doping and temperature changes, primarily due to an increase in electrical conductivity. Additionally, the simultaneous increase in the Seebeck coefficient partially contributes to the improvement.

In order to gain more insights into the thermoelectric properties we deeply investigated the structural, morphological and vibrational properties of the synthesized nanocomposites by XRD, scanning electron microscopy and Raman spectroscopy.

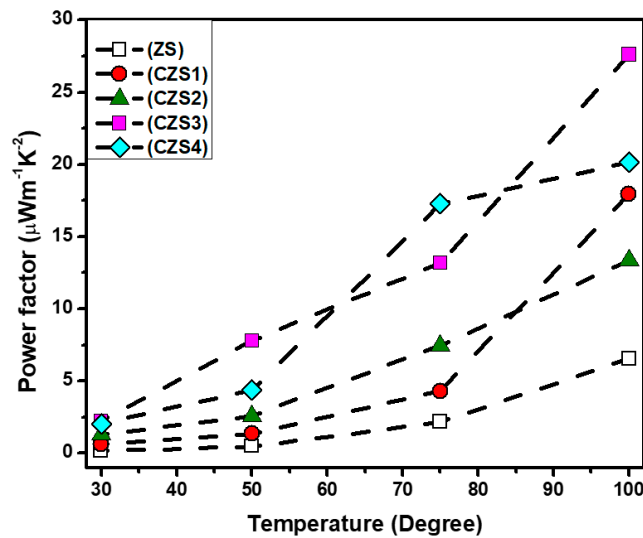


**Figure 2.** Calculated values of the power factor for the undoped and Cu-doped ZnSe samples, as a function of temperature.

### 3.2. Scanning Electron Microscopy

Figure 3 displays scanning electron micrographs of the as-grown samples, revealing that their morphology consists of aggregates of smaller-sized particles. The undoped sample appears relatively compact, with very large aggregates. Meanwhile, the intermediate-doped samples show a similar morphology, with small particles agglomerating into large grains, having sizes ranging from several  $\mu\text{m}$  to tens of microns. Only the sample with the higher doping level exhibits a slightly different morphology, with particles aggregating into almost round-shaped agglomerates with an average size of around  $1\ \mu\text{m}$ .

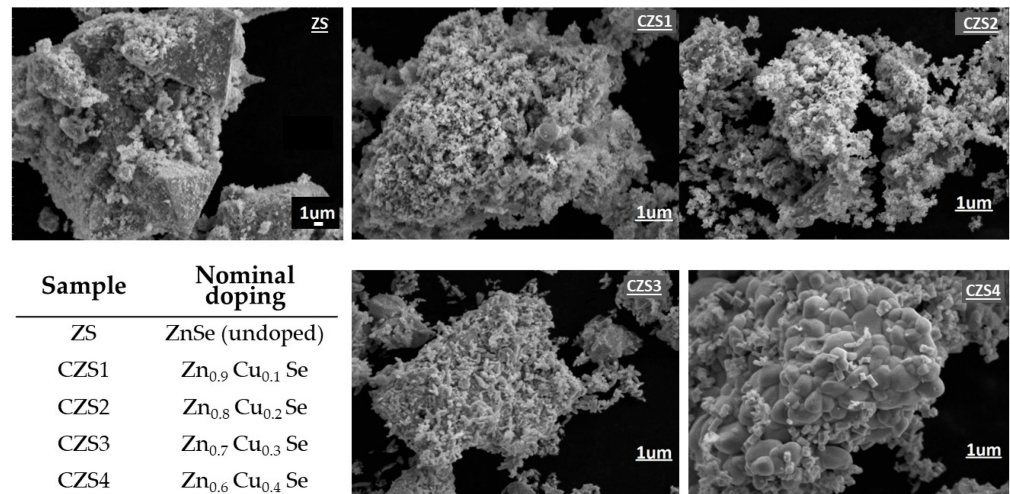


**Figure 3.** Scanning electron micrographs of the prepared  $\text{Cu}^{2+}$  doped ZnSe samples.

### 3.3. X-ray Diffraction

The X-ray diffraction pattern of Cu-doped ZnSe nanoparticles, scanned at  $2\theta$  in the range of  $20\text{--}60^\circ$ , is shown in Figure 4.

The undoped sample (ZS) exhibits well-defined peaks at  $2\theta = 27^\circ$ ,  $45^\circ$ , and  $53^\circ$ . These peaks correspond to diffraction from the (111), (220), and (311) planes in ZnSe with a zinc blende structure (JCPDS File no. 80-0021), which is consistent with previous findings in the literature [30]. Small peaks located at  $23.81^\circ$  and  $39.67^\circ$  are related to the pure zinc and selenium secondary phases [31].

By increasing the Cu concentration the crystallinity of ZnSe nanoparticles decreases, the intensity of the main ZnSe (111) peak decreases and other peaks can be detected. In particular, the additional peaks are located at  $2\theta = 31.81^\circ, 36.29^\circ,$  and  $50.11^\circ$  and are related to the formation of a new CuSe phase in the composite. In particular, peaks at  $31.81^\circ, 36.29^\circ$  and  $50.11^\circ$  correspond to planes (006), (115) and (108), respectively, and correspond to the hexagonal phase of CuSe (JCPDS file no 34-0171) [32,33]. The intensity of these peaks increases as the doping concentration is increased, while the incorporation of Cu in ZnSe, as expected, does not have a strong effect on ZnSe lattice structure as  $\text{Cu}^{2+}$  and  $\text{Zn}^{2+}$  ions have a small ionic radii mismatch [34,35].

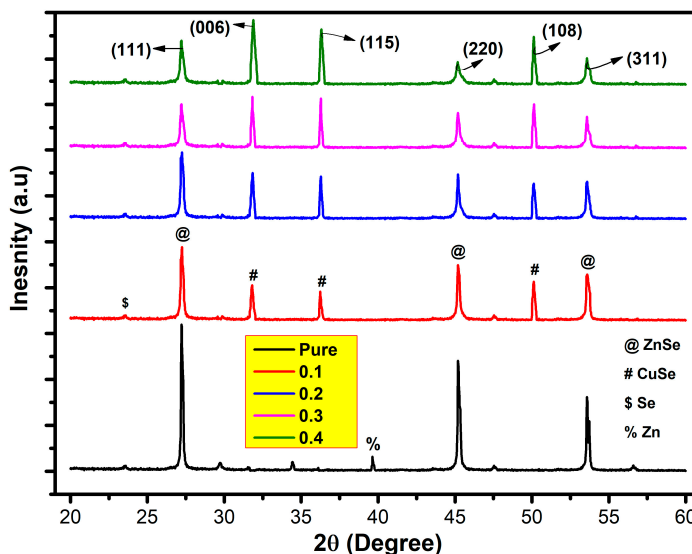


**Figure 4.** XRD patterns of undoped and Fe-doped ZnSe nanoparticles, synthesized using the hydrothermal method.

The grain size was estimated using the Scherrer relation [36,37],  $D = 0.9\lambda / \beta \cos \theta$ , where  $D$  is the crystallite size,  $\beta$  is full width at half maximum of the highest intensity (111) peak,  $\lambda$  is the wavelength of X-ray radiation ( $1.542 \text{ \AA}$  of  $\text{Cu K}\alpha$ ) and  $\theta$  is the Bragg’s angle. The dislocation density ( $\delta$ ), that is the number of defect present in the sample, was calculated using the Williamson and Smallman’s relation [38],  $\delta = 1/D^2$ , and the lattice microstrain was calculated according to the formula  $\epsilon = (\beta \cot(\theta)) / 4$  [39].

Figure 5 reports, as a function of the dopant concentration, the calculated values of the full width at half maximum, of the crystalline size, of the dislocation density and of the microstrain, extracted from the (111) peak of  $\text{Zn}_{1-x}\text{Cu}_x\text{Se}$ .

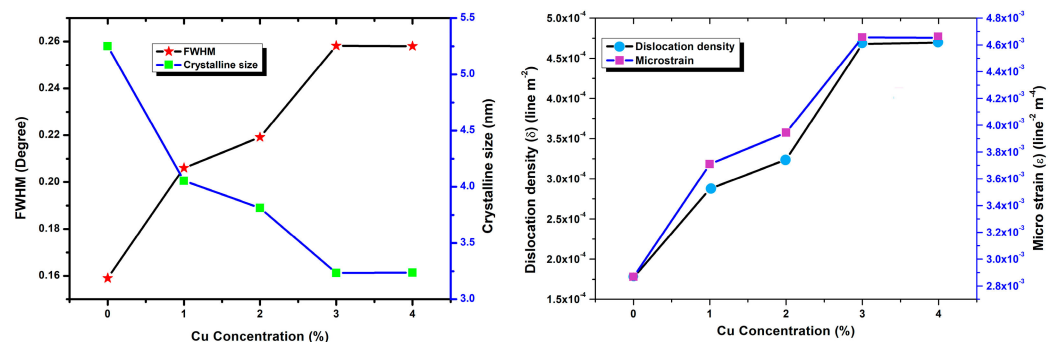


**Figure 5.** (left) Peaks full width at half maximum (FWHM) and crystalline size as a function of the dopants concentration; (right) dislocation density and microstrain as a function of dopants concentration.

As shown in the figure, the undoped sample has a nanocrystalline structure, with a crystalline size about 5.2 nm (Figure 5). The increase of the doping induces an increase in the FWHM and consequently a reduction of crystallinity of doped ZnSe nanoparticles. In particular, the crystalline size decreased monotonically from about 5.2 nm to about 3.2 nm. This reveals the nanocrystalline nature of the material. The results also show that the dislocation density and the microstrain of  $Zn_{1-x}Cu_xSe$  increased as the concentration of copper increased in ZnSe. The presented evidence, especially the decrease in ZnSe crystallinity upon doping, along with the enhanced intensity of the peaks attributed to the secondary CuSe phase, and the increase in defects concentration, suggests that doping plays a role in elevating the significance of grain boundary regions, and that in that regions the secondary CuSe phase is prevalent.

This results shed light on the possible origin of the observed simultaneous increase in Seebeck coefficient and electrical conductivity with increasing temperature, which is not a very common or expected phenomenon but has been reported in the literature several times [28,29]. Previous studies have demonstrated that optimized doping can induce the formation of nanocrystalline structures where the contribution of secondary crystal phases, located at grain boundaries, can be as significant as that of grain regions to the thermoelectric properties [28,40,41]. Indeed, grain boundary engineering has been proposed as a valid tool for enhancing the thermoelectric properties of granular semiconductors [42].

The band structure of the material, the position of the chemical potential, and the carriers' effective mass around grain boundaries can be strongly modified compared to the bulk material. This modification leads to various mechanisms such as the contribution of higher energy carriers to transport and an increase in the electrical conductivity due to an increased scattering mean free path of these carriers. Moreover, energy barriers can form at grain boundaries, promoting an energy filtering effect that enhances the Seebeck coefficient [29], by introducing a strongly energy-dependent scattering mechanism [42].

### 3.4. Raman Spectroscopy

Raman spectroscopy is also a powerful technique for thermoelectric materials characterization as it provides valuable information about their crystal structure, phonon scattering mechanisms, defect density, doping level, and nanostructuring effects [43,44]. The Raman spectroscopy results confirm the information obtained from XRD. Figure 6 shows the Raman spectra of  $Zn_{1-x}Cu_xSe$  at different concentrations of Cu dopant.

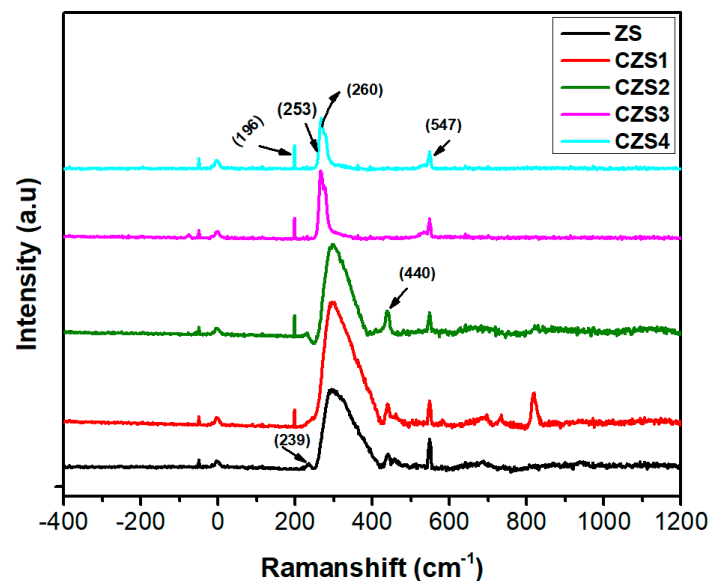


Figure 6. Raman spectra of the undoped and Cu -doped ZnSe samples.

Several series of peaks are observed, including  $239\text{ cm}^{-1}$ ,  $253\text{ cm}^{-1}$ ,  $260\text{ cm}^{-1}$ ,  $440\text{ cm}^{-1}$ , and  $547\text{ cm}^{-1}$ . The peaks at  $253\text{ cm}^{-1}$  and  $547\text{ cm}^{-1}$  were attributed to the longitudinal optical (LO) phonon modes of ZnSe [45]. The intensity of these peaks weakens as copper concentration increases, as copper replaces ZnSe. In the doped samples, the presence of a strong copper selenide phase, which was already detected by XRD analysis, is confirmed by the Raman spectra. Specifically, the intense peak observed at  $196\text{ cm}^{-1}$  in the Raman spectra can be attributed to the Cu-Se vibration (LO) phonon mode of copper selenide, as reported in the literature [46,47]. The peak at  $239\text{ cm}^{-1}$  is attributed to Se-Se extending vibration and can be related to trigonal selenium [47,48].

#### 4. Conclusions

The present study investigated the effect of copper doping on the thermoelectric properties of zinc selenide (ZnSe) nanoparticles synthesized through the hydrothermal method. Five  $\text{Zn}_{1-x}\text{Cu}_x\text{Se}$  samples were prepared, with varying  $\text{Cu}^{2+}$  concentrations from  $x = 0$  to  $x = 0.4$ . Our results demonstrate that Cu doping significantly improves the thermoelectric properties of the ZnSe nanoparticles. Specifically, increasing Cu concentration leads to an increase in the electrical conductivity and Seebeck coefficient of the  $\text{Zn}_{1-x}\text{Cu}_x\text{Se}$  nanocomposites, resulting in enhanced power factors. The structural, vibrational, and morphological properties of the synthesized nanoparticles were investigated using X-ray diffraction, scanning electron microscopy, and Raman spectroscopy, in order to gain more insight into the thermoelectric behavior. The analysis revealed the formation of composites with multiple phases and nanocrystalline morphology. The extracted average grain size was found to be lower than 5 nm and decreased with increasing doping concentration. The observed changes in the structural and morphological properties, particularly the emergence of secondary crystal phases at grain boundaries induced by the dopants, are likely related to the improvement in the thermoelectric properties of the Cu-doped ZnSe nanoparticles. The promising results of this study need to be complemented with further experiments focused on the measurements of the material's thermal conductivity. Our findings provide valuable insights into the underlying mechanisms governing the thermoelectric properties of these nanoparticles and highlight their potential for use in various energy conversion and harvesting applications.

**Author Contributions:** Conceptualization, K.M. and F.R.; data curation, M.I. and N.A.K.; methodology, N.A., K.M. and F.R.; software, M.I., N.A.K. and V.D.; validation, V.D. and N.A.K.; formal analysis, V.D., N.A.K. and M.I.; investigation, M.I., N.A.K. and K.M.; resources, K.M. and F.R.; writing—original draft preparation, V.D.; writing—review and editing, all coauthors; visualization, V.D., M.I. and N.A.K.; supervision, K.M. and F.R.; project administration, N.A., K.M. and F.R.; funding acquisition, K.M. and F.R. All authors have read and agreed to the published version of the manuscript.

**Funding:** This research was funded by the Italian Ministry of Research and Education, PRIN2017 “PELM”, by MIUR-PON, scholarship PhD program “Physics and nano sciences” 2021/22. “Nanotecnologie per la termoelettricità e l’energy harvesting” (Azione IV.5 “Dottorati su tematiche green”) and by the National Recovery and Resilience Plan (NRRP), Mission 04, Component 2 Investment 1.5—NextGenerationEU, Call for Tender No. 3277 dated 30/12/2021. Award Number: 0001052 dated 23 June 2022.

**Data Availability Statement:** Not applicable.

**Conflicts of Interest:** The authors declare no conflict of interest.

#### References

1. Dresselhaus, M.S.; Chen, G.; Tang, M.Y.; Yang, R.; Lee, H.; Wang, D.; Ren, Z.; Fleurial, J.P.; Gogna, P. New Directions for Low-Dimensional Thermoelectric Materials. *Adv. Mater.* **2007**, *19*, 1043–1053. [[CrossRef](#)]
2. Prete, D.; Erdman, P.A.; Demontis, V.; Zannier, V.; Ecolani, D.; Sorba, L.; Beltram, F.; Rossella, F.; Taddei, F.; Roddaro, S. Thermoelectric Conversion at 30 K in InAs/InP Nanowire Quantum Dots. *Nano Lett.* **2019**, *19*, 3033–3039. [[CrossRef](#)] [[PubMed](#)]
3. Chen, R.; Lee, J.; Lee, W.; Li, D. Thermoelectrics of Nanowires. *Chem. Rev.* **2019**, *119*, 9260–9302. [[CrossRef](#)] [[PubMed](#)]

4. Peri, L.; Prete, D.; Demontis, V.; Zannier, V.; Rossi, F.; Sorba, L.; Beltram, F.; Rossella, F. Giant reduction of thermal conductivity and enhancement of thermoelectric performance in twinning superlattice InAsSb nanowires. *Nano Energy* **2022**, *103 Pt A*, 107700. [[CrossRef](#)]
5. Rocci, M.; Demontis, V.; Prete, D.; Ercolani, D.; Sorba, L.; Beltram, F.; Pennelli, G.; Roddaro, S.; Rossella, F. Suspended InAs Nanowire-Based Devices for Thermal Conductivity Measurement Using the  $3\omega$  Method. *J. Mater. Eng. Perform.* **2018**, *27*, 6299. [[CrossRef](#)]
6. Prete, D.; Dimaggio, E.; Demontis, V.; Zannier, V.; Douton, M.-J.R.; Guazzelli, L.; Beltram, F.; Sorba, L.; Pennelli, G.; Rossella, F. Electrostatic Control of the Thermoelectric Figure of Merit in Ion-Gated Nanotransistors. *Adv. Funct. Mater.* **2021**, *31*, 2104175. [[CrossRef](#)]
7. Rahman, M.M.; Das, C.; Rahaman, M.M.; Hussain, K.M.A.; Choudhury, S. Effect of Thickness on Structural, Morphological, and Optical Properties of Copper (Cu) Doped Zinc Selenide (ZnSe) Thin Films by Vacuum Evaporation Method. *J. Bangladesh Acad. Sci.* **2019**, *43*, 159–168. [[CrossRef](#)]
8. Hasaneen, M.F.; Alrowaili, Z.A.; Mohamed, W.S. Structure and optical properties of polycrystalline ZnSe thin films: Validity of Swanepol's approach for calculating the optical parameters. *Mater. Res. Express* **2020**, *7*, 016422. [[CrossRef](#)]
9. Armstrong, S.; Datta, P.; Miles, R. Properties of zinc sulfur selenide deposited using a close-spaced sublimation method. *Thin Solid Films* **2002**, *403–404*, 126–129. [[CrossRef](#)]
10. Nakamura, T.; Fujiwara, S.; Mori, H.; Katayama, K. Novel cladding structure for ZnSe-based white light emitting diodes with longer lifetimes of over 10,000 h. *Jpn. J. Appl. Phys.* **2004**, *43*, 1287. [[CrossRef](#)]
11. Kouklin, N.; Menon, L.; Wong, A.Z.; Thompson, D.W.; Woollam, J.A.; Williams, P.F.; Bandyopadhyay, S. Giant photoresistivity and optically controlled switching in self-assembled nanowires. *Appl. Phys. Lett.* **2001**, *79*, 4423–4425. [[CrossRef](#)]
12. Matsuoka, T. InGaAlN and II–VI Systems for Blue–Green Light-Emitting Devices. *Adv. Mater.* **1996**, *8*, 469–479. [[CrossRef](#)]
13. Choudhury, M.G.M.; Islam, M.R.; Rahman, M.M.; Hakim, M.O.; Khan, M.K.R.; Kao, K.J.; Lai, G.R. Preparation and characterization of ZnSe: Al thin films. *Acta Phys. Slovaca* **2004**, *54*, 417–425.
14. Nweze, C.; Ekpunobi, A.J. Electrodeposition of zinc selenide films on different substrates and its characterization. *Int. J. Sci. Technol.* **2014**, *3*, 201–203.
15. Kumaresan, R.; Ichimura, M.; Arai, E. Photochemical deposition of ZnSe polycrystalline thin films and their characterization. *Thin Solid Film.* **2002**, *414*, 25–30. [[CrossRef](#)]
16. Lokhande, C.; Patil, P.; Ennaoui, A.; Tributsch, H. Chemical bath ZnSe thin films: Deposition and characterisation. *Appl. Surf. Sci.* **1998**, *123–124*, 294–297. [[CrossRef](#)]
17. Islam, A.; Das, C.; Choudhury, S.; Sharmin, M.; Begum, T. Structural and optical characterization of vacuum evaporated zinc selenide thin films. *Eur. Sci. J.* **2014**, *10*, 241–253.
18. Mikulec, F.V.; Kuno, M.; Bennati, M.; Hall, D.A.; Griffin, R.G.; Bawendi, M.G. Organometallic Synthesis and Spectroscopic Characterization of Manganese-Doped CdSe Nanocrystals. *J. Am. Chem. Soc.* **2000**, *122*, 2532–2540. [[CrossRef](#)]
19. Lad, A.D.; Rajesh, C.; Khan, M.; Ali, N.; Gopalakrishnan, I.K.; Kulshreshtha, S.K.; Mahamuni, S. Magnetic behavior of manganese-doped ZnSe quantum dots. *J. Appl. Phys.* **2007**, *101*, 103906. [[CrossRef](#)]
20. Mahamuni, S.; Lad, A.D.; Patole, S. Photoluminescence Properties of Manganese-Doped Zinc Selenide Quantum Dots. *J. Phys. Chem. C* **2008**, *112*, 2271–2277. [[CrossRef](#)]
21. Viswanatha, R.; Battaglia, D.M.; Curtis, M.E.; Mishima, T.D.; Johnson, M.B.; Peng, X. Shape control of doped semiconductor nanocrystals (d-dots). *Nano Res.* **2008**, *1*, 138–144. [[CrossRef](#)]
22. Arandhara, G.; Saikia, P.K. Effect of Cu incorporation on the crystallinity, lattice strain, morphology and electrical properties of nanostructured ZnS-PVA thin films. *Phys. B Condens. Matter* **2021**, *610*, 412924. [[CrossRef](#)]
23. Kumar, P.; Singh, K. Ferromagnetism in Cu-doped ZnSe semiconducting quantum dots. *J. Nanoparticle Res.* **2011**, *13*, 1613–1620. [[CrossRef](#)]
24. Rajesh, C.; Phadnis, C.V.; Sonawane, K.G.; Mahamuni, S. Synthesis and optical properties of copper-doped ZnSe quantum dots. *Phys. Scr.* **2015**, *90*, 15803. [[CrossRef](#)]
25. Jacob, J.; Mahmood, K.; Usman, M.Y.; Rehman, U.; Ali, A.; Ashfaq, A.; Amin, N.; Ikram, S.; Hussain, S. Modulation of thermoelectric properties of bulk ZnAlO by annealing in oxygen environment. *Phys. B Condens. Matter* **2019**, *572*, 247–250. [[CrossRef](#)]
26. Callen, H. *Thermodynamics and an Introduction to Thermostatistics*, 2nd ed.; Wiley: Hoboken, NJ, USA, 1991.
27. Zhang, X.; Yu, K.M.; Kronawitter, C.X.; Ma, Z.; Yu, P.Y.; Mao, S.S. Heavy p-type doping of ZnSe thin films using Cu<sub>2</sub>Se in pulsed laser deposition. *Appl. Phys. Lett.* **2012**, *101*, 042107. [[CrossRef](#)]
28. Liu, J.; Calcabrini, M.; Yu, Y.; Lee, S.; Chang, C.; David, J.; Ghosh, T.; Spadaro, M.C.; Xie, C.; Cojocaru-Mirèdin, O.; et al. Defect Engineering in Solution-Processed Polycrystalline SnSe Leads to High Thermoelectric Performance. *ACS Nano* **2022**, *16*, 78–88. [[CrossRef](#)] [[PubMed](#)]
29. Neophytou, N.; Zianni, X.; Kosina, H.; Frabboni, S.; Lorenzi, B.; Narducci, D. Simultaneous increase in electrical conductivity and Seebeck coefficient in highly boron-doped nanocrystalline Si. *Nanotechnology* **2013**, *24*, 205402. [[CrossRef](#)]
30. Flamee, S.; Dierick, R.; Cirillo, M.; Van Genechten, D.; Aubert, T.; Hens, Z. Synthesis of metal selenide colloidal nanocrystals by the hot injection of selenium powder. *Dalton Trans.* **2013**, *42*, 12654–12661. [[CrossRef](#)]

31. Li, H.; Wang, B.; Li, L. Study on Raman spectra of zinc selenide nanopowders synthesized by hydrothermal method. *J. Alloys Compd.* **2010**, *506*, 327–330. [[CrossRef](#)]
32. Vinod, T.; Jin, X.; Kim, J. Hexagonal nanoplatelets of CuSe synthesized through facile solution phase reaction. *Mater. Res. Bull.* **2011**, *46*, 340–344. [[CrossRef](#)]
33. Barman, B.; Handique, K.; Nanung, Y.; Kalita, P. Synthesis and characterization of chemically synthesized CuSe nanoparticles for photovoltaic application. *Mater. Today Proc.* **2020**, *46*, 6213–6217. [[CrossRef](#)]
34. Beena, V.; Rayar, S.L.; Ajitha, S.; Ahmad, A.; Iftikhar, F.J.; Abualnaja, K.M.; Alomar, T.S.; Ouladsmne, M.; Ali, S. Photocatalytic Dye Degradation and Biological Activities of Cu-Doped ZnSe Nanoparticles and Their Insights. *Water* **2021**, *13*, 2561. [[CrossRef](#)]
35. Ghahramanifard, F.; Rouhollahi, A.; Fazlolahzadeh, O. Electrodeposition of Cu-doped p-type ZnO nanorods; effect of Cu doping on structural, optical and photoelectrocatalytic property of ZnO nanostructure. *Superlattices Microstruct.* **2018**, *114*, 1–14. [[CrossRef](#)]
36. Holzwarth, U.; Gibsong, N. The Scherrer equation versus the ‘Debye-Scherrer equation’. *Nat. Nanotechnol.* **2011**, *6*, 534. [[CrossRef](#)] [[PubMed](#)]
37. Cullity, B.D.; Stock, S.R. *Elementary of X-ray Diffraction, Englewood Cliffs*, 3rd ed.; Prentice-Hall: Hoboken, NJ, USA, 2001.
38. Arshad Javid, M.; Rafi, M.; Ali, I.; Hussain, F.; Imran, M.; Ali, N. Synthesis and study of structural properties of Sn doped ZnO nanoparticles. *Mater. Sci. Poland* **2016**, *34*, 741–746. [[CrossRef](#)]
39. Yon, V.; Rochat, N.; Charles, M.; Nolot, E.; Gergaud, P. X-ray Diffraction Microstrain Analysis for Extraction of Threading Dislocation Density of GaN Films Grown on Silicon, Sapphire, and SiC Substrates. *Phys. Status Solidi B* **2020**, *257*, 1900579. [[CrossRef](#)]
40. Rehman, U.; Jacob, J.; Mahmood, A.; Mahmood, K.; Ali, A.; Ashfaq, A.; Basit, M.; Amin, N.; Ikram, S.; Hussain, S. Modulation of secondary phases in hydrothermally grown zinc oxide nanostructures by varying the Cu dopant concentration for enhanced thermo power. *J. Alloys Compd.* **2020**, *843*, 156081. [[CrossRef](#)]
41. Jacob, J.; Rehman, U.; Mahmood, K.; Ali, A.; Mehboob, K.; Ashfaq, A.; Ikram, S.; Amin, N.; Hussain, S.; Ashraf, F. Improved thermoelectric performance of Al and Sn doped ZnO nano particles by the engineering of secondary phases. *Ceram. Int.* **2020**, *46*, 15013–15017. [[CrossRef](#)]
42. Narducci, D.; Selezneva, E.; Cerofolini, G.; Frabboni, S.; Ottaviani, G. Impact of energy filtering and carrier localization on the thermoelectric properties of granular semiconductors. *J. Solid State Chem.* **2012**, *193*, 19–25. [[CrossRef](#)]
43. Caridad, J.M.; Rossella, F.; Bellani, V.; Grandi, M.S.; Diez, E. Automated detection and characterization of graphene and few-layer graphite via Raman spectroscopy. *J. Raman Spectrosc.* **2011**, *42*, 286–293. [[CrossRef](#)]
44. Bellucci, S.; Chiaretti, M.; Onorato, P.; Rossella, F.; Grandi, M.S.; Galinetto, P.; Sacco, I.; Micciulla, F. Micro-Raman study of the role of sterilization on carbon nanotubes for biomedical applications. *Nanomedicine* **2010**, *5*, 209–215. [[CrossRef](#)] [[PubMed](#)]
45. Hu, Z.D.; Duan, X.F.; Gao, M.; Chen, Q.; Peng, L.-M. ZnSe Nanobelts and Nanowires Synthesized by a Closed Space Vapor Transport Technique. *J. Phys. Chem. C* **2007**, *111*, 2987–2991. [[CrossRef](#)]
46. Minceva-Sukarova, B.; Najdoski, M.; Grozdanov, I.; Chunnillal, C. Raman spectra of thin solid films of some metal sulfides. *J. Mol. Struct.* **1997**, *410–411*, 267–270. [[CrossRef](#)]
47. Sakr, G.; Yahia, I.; Fadel, M.; Fouad, S.; Romčević, N. Optical spectroscopy, optical conductivity, dielectric properties and new methods for determining the gap states of CuSe thin films. *J. Alloys Compd.* **2010**, *507*, 557–562. [[CrossRef](#)]
48. Ramdani, O.; Guillemoles, J.; Lincot, D.; Grand, P.; Chassaing, E.; Kerrec, O.; Rzepka, E. One-step electrodeposited CuInSe<sub>2</sub> thin films studied by Raman spectroscopy. *Thin Solid Films* **2007**, *515*, 5909–5912. [[CrossRef](#)]

**Disclaimer/Publisher’s Note:** The statements, opinions and data contained in all publications are solely those of the individual author(s) and contributor(s) and not of MDPI and/or the editor(s). MDPI and/or the editor(s) disclaim responsibility for any injury to people or property resulting from any ideas, methods, instructions or products referred to in the content.